Nanoscale

Accepted Manuscript

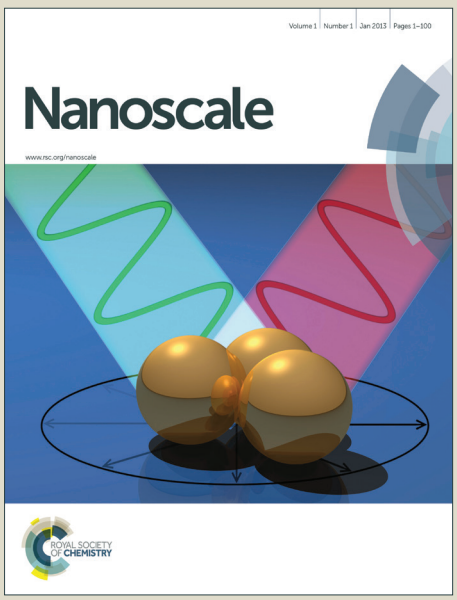

ROYAL SOCIETY OF CHEMISTRY

www.rsc.org/nanoscale

Superior plasmon absorption in iron-doped gold nanoparticles

Vincenzo Amendola,[1,] Rosalba Saija,[2] Onofrio M. Maragò,[3] and Maria Antonia Iatì[3]*

[1]Department of Chemical Sciences, University of Padova, via Marzolo 1, I-35131 Padova, Italy

[2]Dipartimento di Fisica e di Scienze della Terra, Università di Messina, v.le F. Stagno D'Alcontres 31, I-98166 Messina, Italy

[3]CNR-IPCF, Istituto per i Processi Chimico-Fisici, v.le F. Stagno D'Alcontres 37, I-98158 Messina, Italy

* corresponding author: vincenzo.amendola@unipd.it

Abstract

Although the excitation of localized surface plasmons is associated with enhanced scattering and absorption of incoming photons, only the latter is relevant for the efficient conversion of light into heat. Here we show that the absorption cross section of gold nanoparticles is sensibly increased when iron is included in the lattice as a substitutional dopant, i.e. in a gold-iron nanoalloy. Such increase is size and shape dependent, with the best performances observed in nanoshells where a 90-190% improvement is found in a size range that is crucial for practical applications. Our findings are unexpected according to the common believe and previous experimental observations that alloys of Au with transition metals show depressed plasmonic response. These results are promising for the design of efficient plasmonic converters of light into heat and pave the way to more in-depth investigations of plasmonic properties in noble metal nanoalloys.

Keywords: plasmonics, surface plasmon absorption, nanoalloy, nanoparticles, nanoshells

Table of contents text and graph.

Plasmon absorption can be increased up to 200 % just by doping gold nanoparticles (nanospheres, nanoshells, nanordos etc.) with iron. The benefits of alloying Au with Fe are observed in nanostructures larger than 70 - 100 nm and for iron contents of 10 - 20 atomic %. The increment is located in the red and near infrared part of the spectrum, which is the region of interest for most biological applications.

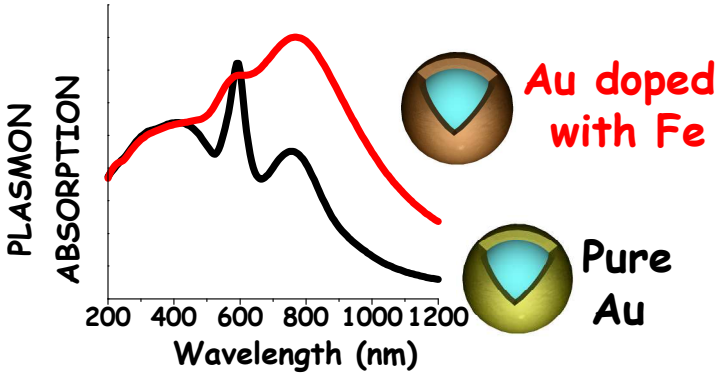

Introduction

Multiple scientific and technological applications rely on the localized surface plasmon resonance (LSPR), which occurs when free electrons in nanoparticles (NPs) are collectively excited by electromagnetic radiation.[1] The highest values known in nature for the extinction cross section (σ_{Ext}) are found in noble metal NPs.[2] Photons exciting plasmons are either absorbed or scattered, and the probability of the two events is determined, respectively, by the NPs absorption (σ_{Abs}) and scattering (σ_{Sca}) cross sections, whose sum gives the σ_{Ext}.[3, 4] Since different properties are associated to scattering and absorption, σ_{Abs} and σ_{Sca} are the relevant quantities for real application of plasmonic NPs.[5-7] Light scattering is an elastic process consisting in the modification of photon propagation direction,[3] therefore NPs with a large σ_{Sca} are preferentially exploited for biolabelling and sensing up to single particle sensitivity,[8] as well as for nanolensing and enhancement of nonlinear optical properties in nearby objects,[9-13] such as plasmonic enhanced near-field absorption in solar cells,[14] surface enhanced Raman scattering[15-17] or plasmonic enhanced third harmonic generation.[18]

Instead, light absorption consists in the transfer of photon energy to the plasmonic nanostructure, where it is rapidly converted to heat.[7] Therefore, NPs with a large σ_{Abs} are suited for photothermal processes such as photothermal therapy,[6, 19, 20] drug release,[21, 22] photoacoustic imaging[8, 23] photothermal contrast imaging,[24, 25] photothermal-induced resonance imaging,[26] photothermal polymerization,[27] plasmonic patterning[28, 29] and light induced vapour generation.[30-32] Another consequence of photon absorption is the alteration of the equilibrium electron Fermi distribution in the metal NP,[33-35] which allows charge injection in the conduction band of nearby semiconductors [33, 36] and it is exploited for plasmon-enhanced catalysis[37, 38] and photocurrent generation.[39, 40]

Since the σ_{Abs} and σ_{Sca} of noble metal NPs grows with, respectively, the 3rd and the 6th power of particle's size,[3, 6] there is a size threshold at which scattering equals absorption.[5, 6] This threshold depends on shape, structure, and composition of NPs,[6, 41] and for noble metal NPs it falls approximately at 60-100 nm.[6, 42, 43] Consequently, absorption for unit mass is maximized by reducing particle size,[42, 43] although in this way the absolute capacity of light-to-heat conversion in the single NP is dramatically diminished.[5, 6, 42, 44] Alternatively, one can choose shape and structure to maximize the absorption cross section.[5, 6, 20] For instance, at equal volume, Au nanorods (NRs) have larger σ_{Abs} than Au nanoshells (NSs) composed by a silica core coated with a gold layer.[5, 6]

In addition to size and structure, the composition of metal NPs is another degree of freedom to maximize plasmon absorption.[9] This controls the complex permittivity, ε, on which σ_{Abs} and σ_{Sca} ultimately depends.[1, 3] Indeed, composition has been seldom considered as a parameter for tuning the plasmonic response of noble metal NPs,[9, 45-49] and there is a relatively low number of noble

metal plasmonic nanoparticles composed by elements different from Au or Ag, such as Pt,[50] Pd,[51] Ga[52] or Al.[53] This is often motivated by the general assumption that other metals cannot perform better than pure Au and Ag nanostructures, either in terms of plasmonic response, ease of synthesis, physical-chemical stability or biocompatibility.[2, 45]

However, the recent interest in magneto-plasmonics[48, 54-56] and plasmon enhanced catalysis[57, 58] pushed to the synthesis of several other plasmonic nanoalloys, beyond the well known Au and Ag nanostructures, such as Au-Fe,[48, 54] Au-Pt[58] and Au-Pd[57] compounds. In these nanosystems, plasmonic performance strongly depends on alloy composition and stoichiometry. In fact, alloying induces the modification of the band structure of the original metals, e.g., by changing the optical gap, moving the Fermi energy and introducing new interband transitions.[45] Generally these alloys exhibit σ_{Ext} and local field enhancement inferior to pure noble metals with identical size and shape,[48, 54, 57, 58] which explains the modest number of studies in which these systems are used for purely plasmonic applications.

Here, we show that alloy NPs composed by a noble metal (Au) doped with 5-15 atomic% (at%) of a transition metal (Fe) have superior absorption cross section than the pure Au counterparts. We start from the experimentally measured optical constants of Au-Fe alloys,[59] in which iron is present as a substitutional dopant in the face centered cubic lattice of gold, to calculate with analytical (Mie theory) and numerical (Discrete Dipole Approximation) methods the dependence of plasmon cross sections on the size and shape of nanostructures. The augmented plasmon absorption in iron-doped Au nanoalloys is prevalently observed in the red and near infrared (NIR) frequencies, which actually is the working window for most photothermal applications.[5, 8] In general, these results suggest that the scarcely investigated field of plasmonic nanoalloys, can be a source of new yet unforeseen solutions for the improvement of plasmonic performances.

Results

Iron-doped gold nanoshells

As a benchmark material for photothermal applications, we first consider Au NSs.[60] In synthetic Au NSs, the scattering cannot be minimized simply by reducing the size of the whole nanostructure, due to experimental difficulties in the control of the thickness of the metal layer.[5, 60] In fact, to obtain a plasmon resonance peaked in the red or NIR, as required in most biological applications of NSs,[8, 60] the gold layer must be small compared to the silica core, and ordinary synthetic approaches usually do not allow a thickness below ca.10nm, unless porous hollow nanostructures such as Au nanocages are preferred.[61] As a consequence, literature usually reports the use of NSs with size above 100nm,[19, 21, 31, 32, 62, 63] whose heating performances are severely limited by the large

scattering contribution.[5, 6, 64] Increasing the σ_{Abs} by acting only on the composition of the metal layer, while maintaining unaltered NS shape and size, would be the preferential strategy to improve the photothermal features of these nanomaterials.[6, 60, 63] Besides, recent studies evidenced that multiple scattering in NSs is useful to concentrate light absorption in very small volumes.[65]

Therefore, by means of Mie theory, we calculated the dependence of σ_{Ext}, σ_{Abs} and σ_{Sca} on the composition of Fe-doped Au alloys, considering a NS with a SiO_2 core of radius 60nm and a 16nm thick metal shell (60,16), inspired by those often described in the literature for photothermal applications (Figure 1).[60, 63, 66] In order to quantitatively compare the plasmonic performances as a function of iron doping, in Figure 1a we report the integrated cross extinction, absorption and scattering sections in the 400-1200nm spectral range (respectively σ_{Ext}[400-1200nm], σ_{Abs}[400-1200nm] and σ_{Sca}[400-1200nm], see also Figure S1 in S.I.), which is the interval where LSPR of NSs are typically observed.[60] The plot of σ_{Ext}[400-1200nm] has a maximum for 100 at% Au, whereas extinction decreases with increasing Fe content, as expected from literature.[48, 54] However, by looking at the two contributions to σ_{Ext} coming from absorption and scattering, we found that σ_{Sca} and σ_{Abs} have two opposite trends. The σ_{Sca} steeply decreases with Fe content, reaching a plateau at 40% of the pure Au value when iron exceeds 25 at%. Instead, the plot of σ_{Abs} shows a remarkable maximum corresponding to 182% of its initial value in proximity of 15 at% of iron, and it is always larger than in the pure Au NS. A similar trend is observed in the plot of the σ_{Ext}, σ_{Abs} and σ_{Sca} values calculated at 800nm (Figure 1b), which is a wavelength frequently exploited for in vivo photothermal applications.[8, 60] In this case, the maximum of σ_{Abs}(800nm) is close to 10 at% of iron, where it is observed an increase of the 190% of the value in pure Au NS. The spectral profiles of σ_{Ext}, σ_{Abs} and σ_{Sca} are compared in Figure 1c-e, showing that the plasmon resonance broadens for increasing Fe doping, in agreement with the recently observed plasmon damping in spherical Au-Fe alloy NPs with different composition.[48, 54] Interestingly, from the $\sigma_{Abs}/\sigma_{Sca}$ ratio reported in Figure 1f, one can see that absorption markedly dominates over scattering in doped Au NSs when the wavelength is longer than 600nm, whereas below this wavelength the trend is inverted and the absorption over scattering ratio is larger in pure Au NSs.

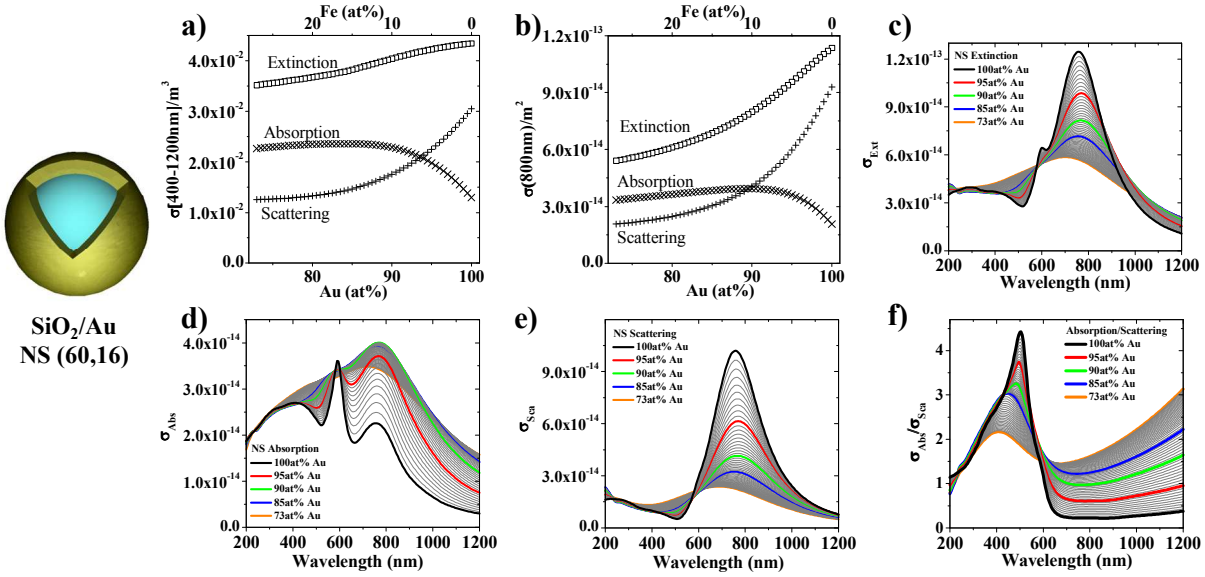

Figure 1. Mie theory calculations of a (60,16) NS in water versus iron doping. (a) σ_{Ext}[400-1200nm], σ_{Abs}[400-1200nm] and σ_{Sca}[400-1200nm]. (b) σ_{Ext}(800nm), σ_{Abs}(800nm) and σ_{Sca}(800nm). (c-f) Spectral dependence of σ_{Ext} (c), σ_{Abs} (d), σ_{Sca} (e) and $\sigma_{Abs}/\sigma_{Sca}$ (f).

In order to confirm the generality of our finding, we calculated the integrated σ_{Abs}[400-1200nm] and the σ_{Abs}(800nm) for a series of NSs with structural parameters extracted from literature[19, 21, 31, 32, 60, 62, 63, 66] (Figure 2a-b and S2 in S.I.), focusing on four representative levels of iron doping (0, 5, 10 and 15 at% Fe). We found that the calculated plasmon absorption is systematically larger in the doped Au nanostructures, with an improvement reaching a remarkable +190% in the (60,22) NS. Such an increase of σ_{Abs} can prove useful to minimize damage of healthy tissues in photothermal therapy,[60] as well as to increase the minimum detectable amount of NSs in photothermal imaging techniques.[63] In general, such an improvement would allow the reduction of the dose of nanomaterials administered for theragnostic purposes, which is important for the minimization of side effect related to long term accumulation of the nanodrugs.[60, 63]

Since (60,12) NSs have been applied also to vapour generation by conversion of sunlight into heat,[30-32] the more appropriate parameter to evaluate the photothermal performances for such a specific application is the convolution of the solar spectral irradiance at air mass 1.5 (AM1.5) with the σ_{Abs}.[30-32] In this case (see Figure 2c), a remarkable improvement of 40% in the light-to-heat

conversion is predicted in the 280-1200nm wavelength range by doping the Au shell with 10 at% of Fe.

In figs. 2d-g we further investigate the effect of Fe doping as a function of the structural parameters of NSs, such as size and shell thickness (see also figs. S3-S4). When the shell thickness exceeds 10nm, the σ_{Abs}[400-1200nm] and the σ_{Abs}(800nm) of doped shells surmount by more than 50% that of pure Au NSs for increasing shell thickness and a fixed diameter of 140nm (Figure 2d-e and S3). As stated before, this is equivalent to the smallest thickness found in literature.[60] Interestingly, when σ_{Abs}[400-1200nm] is plotted versus NSs diameter (Figure 2f), while maintaining unaltered the ratio of core-to-shell thickness at 4:1, we observe that iron-doped NSs have superior absorption only when size exceeds the threshold value of 100nm. A different behaviour is observed for the value of σ_{Abs} at 800nm (Figure 2e), which is larger in Fe-doped NSs in the whole range of diameters considered, with an increase of +50% already for a size of 70nm. Indeed, the spectral profiles of σ_{Abs} (Figure S4 in S.I.) show increasing bandwidth for increasing Fe-doping, which is the main reason for the superior σ_{Abs}(800nm) of doped NSs with size below 100nm, but only above this threshold the σ_{Abs} of alloy NSs becomes larger than pure Au NSs in the whole red-NIR spectral range.

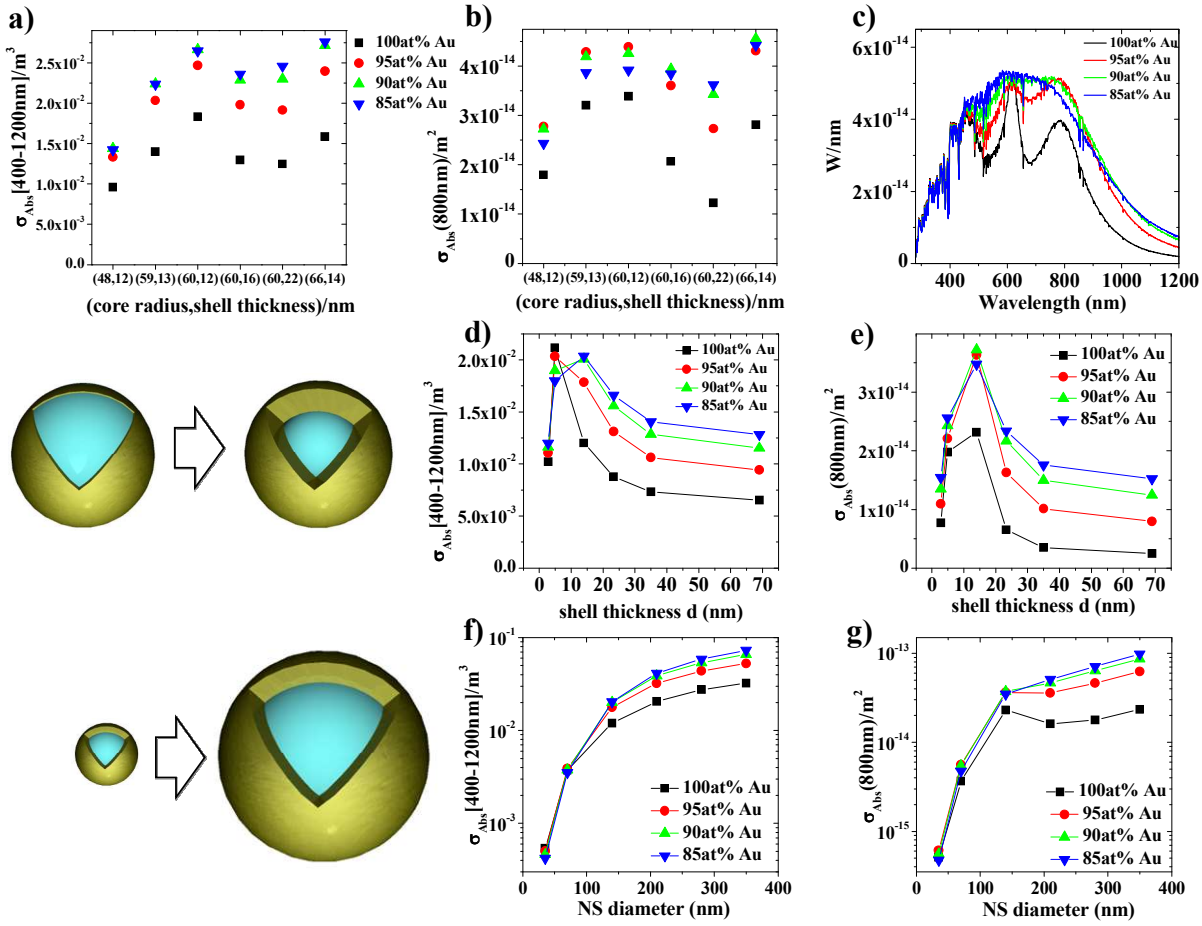

Figure 2. σ_{Abs}[400-1200nm] (a) and σ_{Abs}(800nm) (b) for four representative levels of iron doping (0at%Fe-100at%Au in black squares, 5at%Fe-95at%Au in red circles, 10at%Fe-90at%Au in green triangles, 15at%Fe-85at%Au in blue triangles) in a series of NSs with structural parameters extracted from literature (for details see text). (c) Convolution of σ_{Abs} with the solar spectral AM1.5 irradiance. (d-e) Variation of σ_{Abs}[400-1200nm] (d) and σ_{Abs}(800nm) (e) in a NS with a constant diameter of 140nm and variable shell thickness. (f-g) Variation σ_{Abs}[400-1200nm] (f) and σ_{Abs}(800nm) (g) in a NS with constant ratio of core to shell of 4:1 and variable diameter.

Role of shape: spheres, dimers, and nanorods

The effect of iron-doping was investigated further by considering other shapes exploited for photothermal applications, such as compact spheres, sphere dimers and nanorods (Figure 3 and S5-S8 in S.I.). In the case of compact spheres, the plot of σ_{Abs}[400-1200nm] versus size for the four representative levels of iron-doping reported in Figure 3a shows that Au-Fe NPs absorb 100% more than Au NPs when particles are bigger than 100nm. The σ_{Abs}(800nm) of the alloy is larger than in Au NPs in the whole range of size considered (Figure 3b), although this is again related to the plasmon bandwidth in doped particles with diameter below 70nm (see Figure S5 in S.I.). Instead, the σ_{Abs} of alloys becomes superior in the whole spectral range only for sizes exceeding 70nm.

Surprisingly, the beneficial effect of iron doping on plasmon absorption is less conspicuous in a dimer of spheres separated by a 1nm gap (Figure 3c-d). The plot of σ_{Abs}[400-1200nm] versus sphere's diameter shows a maximum increment of +30% for 140nm alloys, with only a slight increment when the iron-doped nanospheres exceed 70nm (Figure 3c and S6a). The trend of σ_{Abs}(800nm) reflects that of monomers (Figure 3d), with the best absorption increment (+80%) observed in Au-Fe dimers larger than 100nm, whereas the behaviour at lower size is dominated by the dependence of plasmon bandwidth on iron-doping (see Figure S6b-h in S.I.).

The case of NRs with hemispherical caps can help obtaining more insights about the difference between isolated and coupled nanospheres (Figure 3e-h and S7-S8). In fact, NRs have elongated shape and plasmon resonances in the red and NIR,[6] similarly to sphere's dimers. At the same time, isolated NRs are not subjected to the enormous local field enhancement typically observed at the hot spots in the junction between two plasmonic nanospheres.[15] For an easier comparison of NRs with nanospheres, dimers and NSs, we considered the effective size d_{eff}, defined as the diameter of the equi-volume sphere.[6, 43] In case of a NR with a major to minor axis ratio (aspect ratio) of 2.5 and incident electric field polarized along the major axis, we found that the σ_{Abs}[400-1200nm] of Au-Fe alloys is up to 150% larger than in pure Au when d_{eff} is larger than 70nm (Figure 3e and S7). Similarly, σ_{Abs}(800nm) of iron-doped NRs exceeds by 70-380% that of pure Au rods (Figure 3f).

To better elucidate the influence of the shape on the absorption performances of iron-doped alloys, we also investigated the effect of rod's aspect ratio in the range from 1.5 to 5.5, while maintaining unchanged d_{eff} at 110nm. For the whole range of aspect ratios, doped NRs have superior absorption performances (Figure 3g-h and S8), suggesting that particle geometry is less important than size.

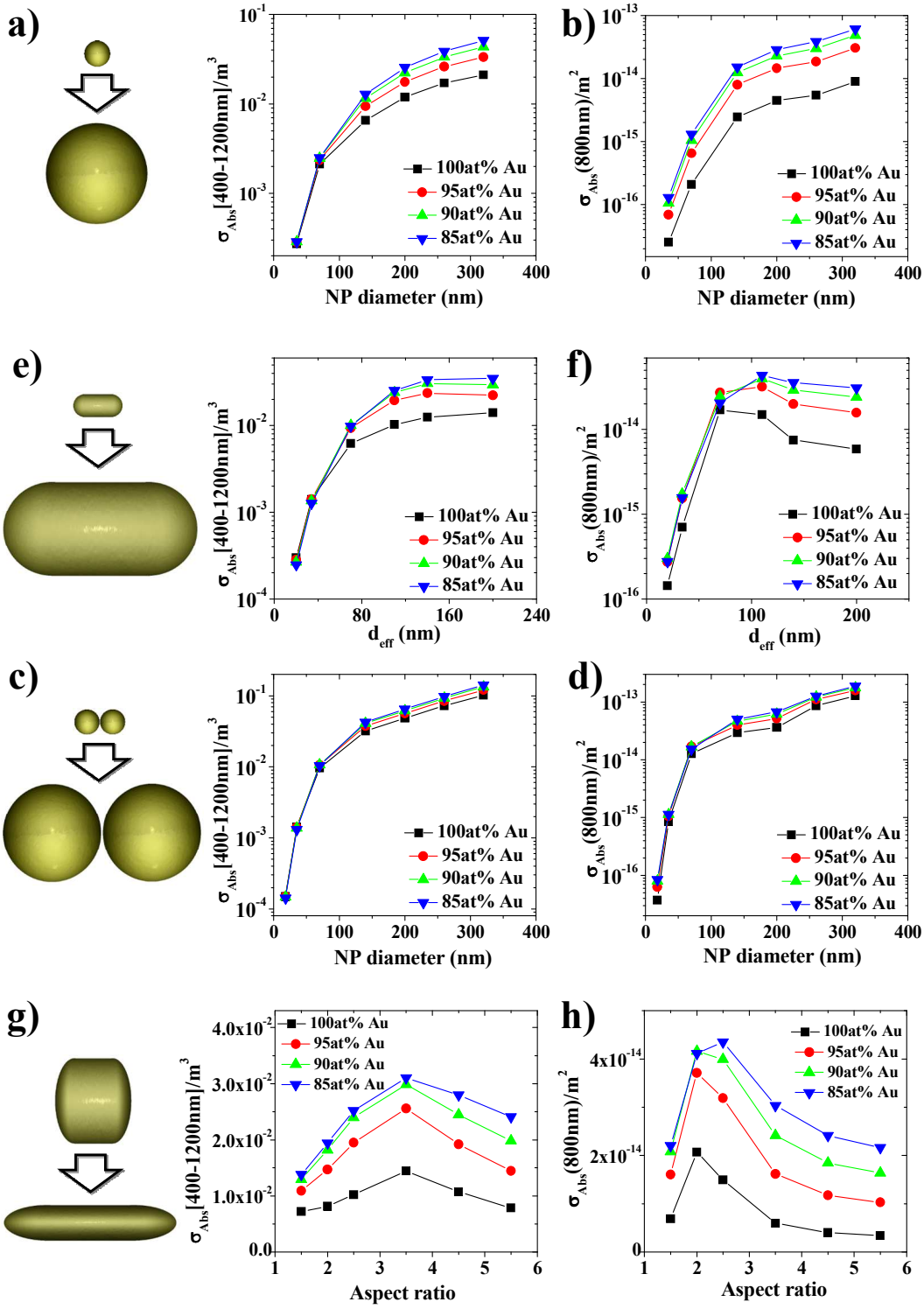

Figure 3. (a-b) σ_{Abs}[400-1200nm] (a) and σ_{Abs}(800nm) (b) in nanospheres with different size. (c-d) σ_{Abs}[400-1200nm] (c) and σ_{Abs}(800nm) (d) in a dimer of nanospheres with different size and interparticle gap of 1nm. (e-f) σ_{Abs}[400-1200nm] (e) and σ_{Abs}(800nm) (f) in NRs with aspect ratio of 2.5 and different effective size. (g-h) σ_{Abs}[400-1200nm] (g) and σ_{Abs}(800nm) (h) in NRs with variable aspect ratio and constant effective size of 110nm.

Discussion

Overall, our calculations show that plasmon absorption is sensibly improved in iron-doped Au nanostructures larger than 70-100nm. Below this size threshold, the benefits of iron doping on the σ_{Abs} are minimal and prevalently observed in the NIR as a consequence of plasmonic band broadening in Au-Fe alloy NPs. The change of σ_{Abs} originates from the modification of the optical constants of gold after doping with iron. Previous experimental studies on the optical properties of thin AuFe alloy films[59] and nanospheres[48, 54] showed that doping Au with Fe introduces new single electron transitions, which are generated by electrons lying in the iron d-states below the Fermi surface of the metal. In general, low-frequency interband transitions are observed when noble metals and transition metals with partially occupied d-states are alloyed together.[45, 59, 67] These low-energy transitions favour the rapid decay of the plasmon excitation into electron-hole pairs,[45] thus being the main cause for plasmon band broadening in Au-Fe alloys.[48, 54] This effect increases with the concentration of the transition metal in the alloy.[48, 59] Moreover, Fe has a smaller atomic number than Au, meaning that the overall electronic structure of the alloy is different compared to pure Au.[45, 59, 68] For these reasons, iron doping modifies the band structure of the metal and the resulting optical permittivity, in particular by decreasing its real component (ε') and increasing its imaginary part (ε") in comparison to pure Au (see Figure 4a-b).

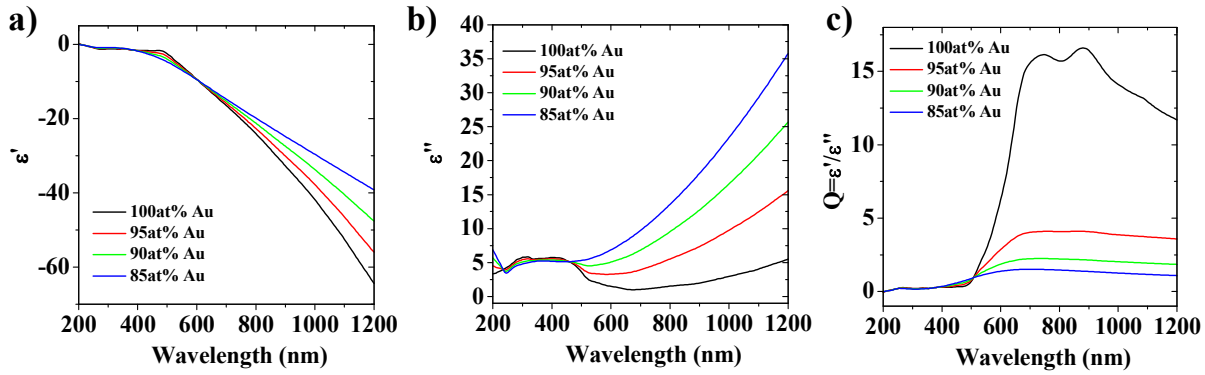

Figure 4. Real (a) and imaginary (b) part of the optical constant for four representative levels of iron doping (0at%Fe-100at%Au in black, 5at%Fe-95at%Au in red, 10at%Fe-90at%Au in green, 15at%Fe-85at%Au in blue). (c) The plasmonic quality factor Q for the same four compositions.

The effect of iron-doping on the plasmonic absorption of Au nanostructures can be explained by considering the dependence of σ_{Abs} for a generic NP at the photon frequency ω:[43, 69, 70]

$$\sigma_{Abs}(\omega) = \frac{k}{\varepsilon_0 \left| E_0^2 \right|} \varepsilon'' \int_{NP} \left| E_{NP}^2 \right| dV_{NP} \qquad (1)$$

where E_0 is the electric field of the incident light, measured in the medium surrounding the NP of volume V_{NP}, ε_0 is the vacuum dielectric permittivity and E_{NP} is the electric field of the electromagnetic radiation inside the NP. On the one hand, $\sigma_{Abs}(\omega)$ is proportional to the lossy part of the optical constant ε", which is augmented by iron doping (see Figure 4b). On the other hand, $\sigma_{Abs}(\omega)$ is proportional to the square of the electric field E_{NP} inside the NP, which is maximized when the quality factor Q of the plasmon resonance is maximum.[69, 70] Following Blaber,[70] the plasmonic performances of metals with different composition can be compared, independent of particle geometry, assuming that Q=-ε'/ε". In Figure 4c we report Q for the same four representative Au-Fe compositions of Figures 2-3, and we clearly found that Q is largest in pure Au. This is in agreement with the fact that highest σ_{Ext} are systematically obtained for Au NPs rather than Au-Fe alloys (see, e.g., Figure 1). Therefore, iron doping has the two opposite effects of increasing ε" and decreasing E_{NP}, and the Au-Fe alloys have superior σ_{Abs} only when the ε" contribution prevails over $\left|E_{NP}^2\right|$ in eq. 1. It is important to point out that, in addition to composition, E_{NP} depends also on particle shape, size and assembly,[70] and it is not uniform throughout the NPs volume.[45, 71] In particular, the value of E_{NP} in proximity of small gaps in assemblies of nanoparticle is several orders of magnitude larger than in isolated nanoparticles.[69, 70] Indeed, the gaps between NPs are also called hot spots because of this strong electromagnetic field enhancement,[15] and this is the region where the conversion of light into heat is maximum.[69, 71] In order to further investigate this point, we calculated, using the multipole fields expansion,[4, 72, 73] the internal electric field and mapped $\left|E_{NP}^2\right|$ in spheres (Figure 5a), nanoshells (Figure 5b) and sphere dimers (Figure 5b) at the wavelength where plasmon absorption is maximum. In particular, we compared the two opposite cases of pure Au and Au(85)Fe(15) NPs and we considered two distinct sizes corresponding to spheres with diameter of 35nm and 140nm, i.e. below and above the threshold for the amplification of plasmon absorption in iron doped NPs. Results confirm that $\left|E_{NP}^2\right|$ is always larger in pure Au NPs than in the Fe-Au alloy, although the difference is more evident for 35 nm NPs and for dimers of nanospheres. Besides, one must observe that the maximum of absorbance red shifts for increasing NPs' size, moving to the region where ε" of the alloy is larger and can compensate the loss in the $\left|E_{NP}^2\right|$ term. These two trends explain why the superior plasmon absorption is observed in isolated NPs with size above ~70 nm such as NSs, nanospheres and NRs, rather than in a dimer of spheres or NPs with size below ~70 nm, where E_{NP} is the dominant contribution.[15] We expect this trend to be general for all the shapes where the local field enhancement is remarkable, such as in all the coupled nanostructures and particles with sharp tips, corners or edges.

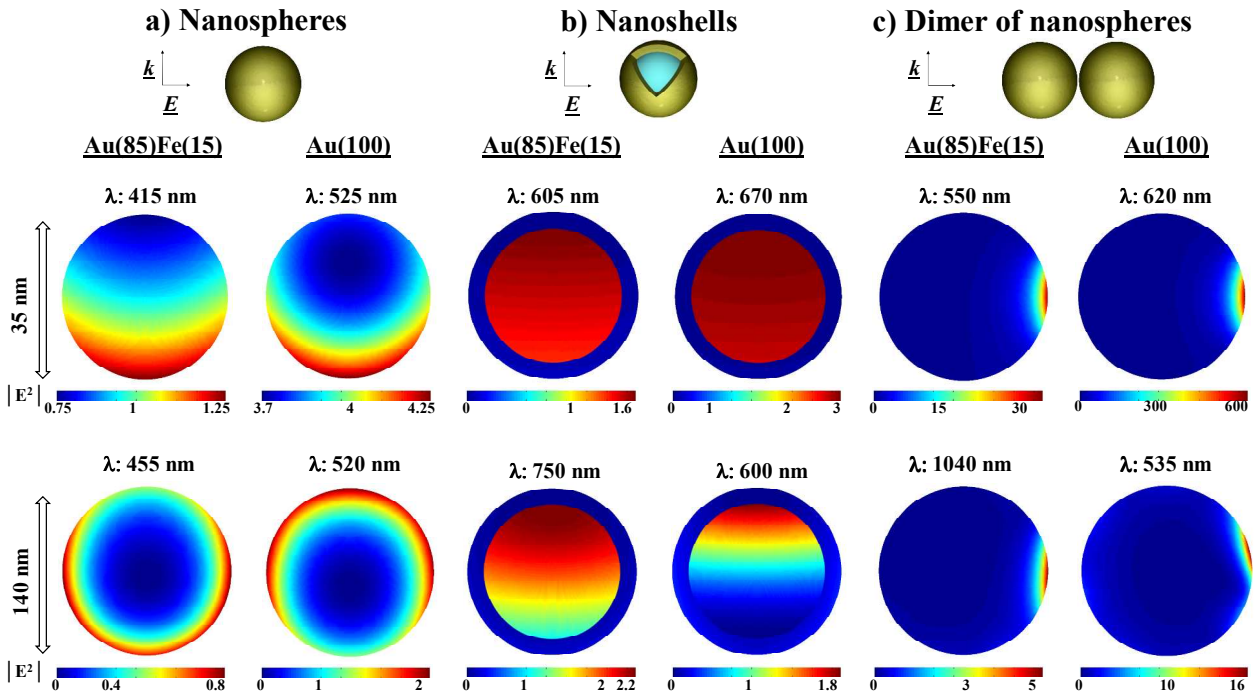

Figure 5. Map of the internal electric field $|E^2|$ in nanostructures of differents shape (a: nanosphere; b: nanoshells; c: dimer of nanospheres), composition (pure Au or Au(85)Fe(15)), and diameter (35 nm or 140 nm). Calculations are performed for incident monocromatic radiation at the wavelength were the maximum absorption occurs (as indicated in the figure). The incident electric field of the electromagnetic radiation is parallel to the plane of the map. Due to the symmetry of the dimer of nanospheres, only the left side particle is shown.

For what concern the role played by the type of dopant in the Au alloy, a quantitative comparison with other transition elements would be possible by using the experimentally measured optical constants of each compound, as done for the AuFe system in a range of compositions.[48, 54, 59] However, these data are available only for a limited number of Au alloys containing other noble metals such as Ag, Cu, Pt or Pd,[74] for which no absorption enhancement has been observed in the past.[9, 45] In all the other cases, the synthesis of the alloy and the ellipsometric investigation of the optical constants as a function of the composition would be necessary to foresee the plasmonic properties. In fact, as shown in Figure S10 of the S.I., the extrapolation of alloys optical constants from that of pure metals in the absence of an experimental checkpoint is unreliable. However, we know from literature that electrons lying in d-states of Fe dopants below the Fermi level play a major role in the modification of AuFe alloy band structure, by enabling low-frequency interband transitions.[59, 67] On the basis of similar observations on the band structure of other Au alloys,[45, 75] we expect that an increased plasmon absorption may be possible also by doping Au with other

transition metals with partially filled d-orbitals such as, for instance, Cr, Co and, to a lower extent, Ni. In case of transition metals such as Pd or Pt, whose d-orbitals are almost (Pd) or completely (Pt) occupied, not such a modification of the Au band structure has been observed in the red or NIR.[76-79] Conversely, an increased absorbance in the UV-visible range due to single-electron transitions from d-states in Pt and Pd, and a simultaneous damping of plasmon absorption, have been reported.[45, 57, 58, 76-79] This can be explained with the decrease of the real part (ε') of the optical constant of the alloy containign Pd or Pt, and a modest increase of its imaginary part (ε'') at visible frequencies, compared to pure Au.[45, 80] In general, this suggests that elements with occupied d-states are not suitable for the increase of plasmon absorption in Au alloys.

Conclusion

In summary, we showed that iron-doped Au nanostructures with size above 70-100nm have superior absorption cross section than pure Au counterparts. In particular, a remarkable increase of 90-190% is predicted in NSs and nanospheres commonly exploited for photothermal applications. The effect is explained with the modification of the band structure of gold after doping with iron, with consequent increase of the lossy part of the optical constant. These results are general, suggesting that the band structure of noble metals can be engineered by doping with the appropriate combination of transition metals to obtain optimized plasmonic properties. At the moment, the optical constants of noble metal alloys containing one or more transition metals are in large part unknown, therefore the real potential of doping for the improvement of plasmonic performances is unexplored, and other transition metals, amongst those miscible with Au, could perform better than iron. Overall, this study foster the interest on the scarcely investigated field of noble metal nanoalloys, which can be a source of new unforeseen solutions for the improvement of plasmonic performances.

Methods

Mie theory for compact spheres.

The extinction, scattering and absorption cross-sections of spherical nanoparticles (σ_{Ext}, σ_{Sca} and σ_{Abs}) were calculated using the Mie model for compact spheres:[1, 3]

$$\sigma_{Ext} = \frac{2\pi}{\left|\bar{k}^2\right|}\sum_{L=1}^{\infty}(2L+1)\mathrm{Re}[a_L + b_L] \qquad \text{(m1)}$$

$$\sigma_{Sca} = \frac{2\pi}{\left|\bar{k}^2\right|}\sum_{L=1}^{\infty}(2L+1)\left(Abs[a_L]^2 + Abs[b_L]^2\right) \qquad \text{(m2)}$$

$$\sigma_{Abs} = \sigma_{Ext} - \sigma_{Sca} \quad \text{(m3)}$$

$$a_L = \frac{m\cdot\psi_L(mx)\cdot\psi_L'(x) - \psi_L'(mx)\cdot\psi_L(x)}{m\cdot\psi_L(mx)\cdot\eta_L'(x) - \psi_L'(mx)\cdot\eta_L(x)} \quad \text{(m4)}$$

$$b_L = \frac{\psi_L(mx)\cdot\psi_L'(x) - m\psi_L'(mx)\cdot\psi_L(x)}{\psi_L(mx)\cdot\eta_L'(x) - m\psi_L'(mx)\cdot\eta_L(x)} \quad \text{(m5)}$$

$$m = \frac{n(R)}{n_m} \quad \text{(m6)}$$

$$x = \left|\bar{k}\right| R\,, \quad \text{(m7)}$$

where R is the sphere radius, k is the incident photon wavevector in the host matrix with refractive index n_m, Ψ_L and η_L are the spherical Riccati-Bessel functions, and $n(R)$ is the complex refractive index of the sphere. In all calculations, the highest multipolar order (L) considered was 3 and n_m = 1.334 (water matrix).

Mie theory for core-shell spheres.

The extinction, scattering and absorption cross-sections of NSs were calculated using the generalization of the Mie model for multilayer spheres:[1]

$$\sigma_{ext} = \frac{2\pi}{\left|\bar{k}_h^2\right|}\sum_{L=1}^{\infty}(2L+1)\,\mathrm{Re}\left[a_L + b_L\right] \quad \text{(m8)}$$

$$\sigma_{Sca} = \frac{2\pi}{\left|\bar{k}_h^2\right|}\sum_{L=1}^{\infty}(2L+1)\left(Abs\left[a_L\right]^2 + Abs\left[b_L\right]^2\right) \quad \text{(m9)}$$

$$\sigma_{Abs} = \sigma_{Ext} - \sigma_{Sca} \quad \text{(m10)}$$

$$a_L = \frac{m_r\cdot\psi_L(m_r x_r)\cdot\left[\psi_L'(x_r) + T_L^r\chi_L'(x_r)\right] - \psi_L'(m_r x_r)\cdot\left[\psi_L(x_r) + T_L^r\chi_L(x_r)\right]}{m_r\cdot\eta_L(m_r x_r)\cdot\left[\psi_L'(x_r) + T_L^r\chi_L'(x_r)\right] - \eta_L'(m_r x_r)\cdot\left[\psi_L(x_r) + T_L^r\chi_L(x_r)\right]} \quad \text{(m11)}$$

$$b_L = \frac{\psi_L(m_r x_r)\cdot\left[\psi_L'(x_r) + S_L^r\chi_L'(x_r)\right] - m_r\cdot\psi_L'(m_r x_r)\cdot\left[\psi_L(x_r) + S_L^r\chi_L(x_r)\right]}{\eta_L(m_r x_r)\cdot\left[\psi_L'(x_r) + S_L^r\chi_L'(x_r)\right] - m_r\cdot\eta_L'(m_r x_r)\cdot\left[\psi_L(x_r) + S_L^r\chi_L(x_r)\right]} \quad \text{(m12)}$$

$$T_L^s = -\frac{m_s\cdot\psi_L(m_s x_s)\cdot\left[\psi_L'(x_s) + T_L^{s-1}\chi_L'(x_s)\right] - \psi_L'(m_s x_s)\cdot\left[\psi_L(x_s) + T_L^{s-1}\chi_L(x_s)\right]}{m_s\cdot\chi_L(m_s x_s)\cdot\left[\psi_L'(x_s) + T_L^{s-1}\chi_L'(x_s)\right] - \chi_L'(m_s x_s)\cdot\left[\psi_L(x_s) + T_L^{s-1}\chi_L(x_s)\right]} \quad \text{(m13)}$$

$$T_L^1 = -\frac{m_1\cdot\psi_L(m_1 x_1)\cdot\psi_L'(x_1) - \psi_L'(m_1 x_1)\cdot\psi_L(x_1)}{m_1\cdot\chi_L(m_1 x_1)\cdot\psi_L'(x_1) - \chi_L'(m_1 x_1)\cdot\psi_L(x_1)} \quad \text{(m14)}$$

$$S_L^s = -\frac{\psi_L(m_s x_s)\cdot\left[\psi_L'(x_s) + S_L^{s-1}\chi_L'(x_s)\right] - m_s\cdot\psi_L'(m_s x_s)\cdot\left[\psi_L(x_s) + S_L^{s-1}\chi_L(x_s)\right]}{\chi_L(m_s x_s)\cdot\left[\psi_L'(x_s) + S_L^{s-1}\chi_L'(x_s)\right] - m_s\cdot\chi_L'(m_s x_s)\cdot\left[\psi_L(x_s) + S_L^{s-1}\chi_L(x_s)\right]} \quad \text{(m15)}$$

$$S_L^1 = -\frac{\psi_L(m_1 x_1)\cdot\psi_L'(x_1) - m_1\cdot\psi_L'(m_1 x_1)\cdot\psi_L(x_1)}{\chi_L(m_1 x_1)\cdot\psi_L'(x_1) - m_1\cdot\chi_L'(m_1 x_1)\cdot\psi_L(x_1)} \quad \text{(m16)}$$

$$m_s = \frac{n_{s+1}}{n_s} \quad \text{(m17)}$$

$$x_s = \left|\bar{k}_s\right| R_s \quad \text{(m18)}$$

where $\chi(x)$ is one of the spherical Riccati – Bessel functions, k_h is the wavenumber of the incident photons calculated in the host matrix, and s is the layer number, ranging from 1 (the core) to $r + 1$ (the surrounding matrix with refractive index n_m), with r total number of layers (1 in the Au NSs case). In all calculations, the highest multipolar order (L) considered was 3 and $n_{s+1} = n_m = 1.334$ (water matrix).

Maps of internal fields.

The maps of the internal electric field intensity, $\left|E_{NP}^2\right|$, in nanospheres, nanoshells, and dimers of nanospheres are obtained through the solutions of the same boundary conditions equations defining the Mie expansion coefficients. For the case of dimers, we use the addition theorem for vector spherical harmonics,[72] that enables the solution of the scattering problem also for clusters of any size, shape, and composition and the retrieval of the relevant amplitudes for scattered and internal fields.[4, 73]

Discrete-Dipole Approximation method.

Calculations of the extinction cross section of nanosphere dimers and NRs were performed by the DDA method.[81] In DDA, the structure of interest, usually called "target", is composed by a cubic array of N polarizable points (i.e. N cubic dipoles). The polarization P_j induced on each dipole j of position r_j and polarizability p_j is given by:[81]

$$\bar{P}_j = p_j \bar{E}_{Loc}\left(\bar{r}_j\right) \quad \text{(m19)}$$

where E_{Loc} is the electric field originated by the incident radiation, which includes the contribution of all other dipoles:[81]

$$\bar{E}_{Loc}\left(\bar{r}_j\right) = \bar{E}_0 \exp\left(i\bar{k}\cdot\bar{r}_j + i\omega t\right) - \sum_{l\neq j} \bar{\bar{A}}_{jl}\bar{P}_l \quad \text{(m20)}$$

where $\bar{\bar{A}}_{jl}$ is the interaction matrix. The full expression of $\bar{\bar{A}}_{jl}\bar{P}_l$ is:[81]

$$\bar{\bar{A}}_{jl}\bar{P}_l = \frac{\exp\left(ik\bar{r}_{jl}\right)}{\bar{r}_{jl}^{\,3}} \times \left\{ k^2 \bar{r}_{jl} \times \left(\bar{r}_{jl} \times \bar{P}_l\right) + \frac{\left(1 - ik\bar{r}_{ij}\right)}{\bar{r}_{jl}^{\,2}} \left[\bar{r}_{jl}^{\,2}\bar{P}_l - 3\bar{r}_{jl}\left(\bar{r}_{jl}\cdot\bar{P}_l\right)\right] \right\} \quad \text{(m21)}$$

An important part of DDA is the use of an appropriate expression for p_i.[81, 82] The most applied expression was developed by Draine and Goodman[82] as a correction of the Clausius - Mossotti polarizability by a series expansion of kd and ε_m, where d is the interdipole spacing. This expression

was used for our calculations, performed by the software DDSCAT 7.1. More than 10^5 dipoles were used for each target, as required to reduce computational errors well below 10%.[41, 81, 82] A matrix with refractive index of 1.334 was used in all cases.

Optical constants.

The experimental optical constants of Au, $Au_{84}Fe_{16}$ and $Au_{73}Fe_{27}$ were taken from literature (ref.[74] and [59]) and are reported in Figure S8. For all the other values, we used the linear averaging of the optical constants of the two alloys with the closest composition, according to a successful protocol previously published and validated by comparison with experiments.[41, 48, 54, 83]

The optical constants were corrected for size effects,[1, 41, 84] as reported previously.[41, 48, 54, 84] We adopted a size corrected dielectric constant to account for the intrinsic size effect, which is important when the mean free path of conduction electrons becomes comparable to particles size l along the direction of polarization promoted by the electromagnetic field. In the assumption that only the free electron behaviour is affected by the size of nanoparticles, $\varepsilon(\omega,l)$ can be expressed in the following way:[1, 41, 84]

$$\varepsilon(\omega,l)=\varepsilon_{\infty}(\omega)+\left[{\omega_P}^2\left(\frac{1}{\omega^2+{\Gamma_{\infty}}^2}-\frac{1}{\omega^2+\Gamma(l)^2}\right)\right]+i\left[\frac{{\omega_P}^2}{\omega}\left(\frac{\Gamma(l)}{\omega^2+\Gamma(l)^2}-\frac{\Gamma_{\infty}}{\omega^2+{\Gamma_{\infty}}^2}\right)\right] \qquad \text{(m22)}$$

where $\varepsilon_{\infty}(\omega)$ is the dielectric function of bulk metal at frequency ω, $\Gamma(l)$ is the l-dependent free electrons relaxation frequency and Γ_{∞} is the bulk metal value. $\Gamma(l)$ is expressed according to a size equation:[1, 41, 84]

$$\Gamma(l)=\Gamma_{\infty}+A\frac{v_F}{l} \qquad \text{(m23)}$$

where v_F is the electron's Fermi velocity and A is an empirical parameter set equal to 1 in all cases. Equation (m23) suggests that the damping frequency of NPs with anistropic shape depends on particle orientation, because l is different for plasmonic oscillations along different directions.[1, 41, 84] However, what is really important for the right determination of Γ is the ratio A/l and not only the value of l. Moreover, the charge distribution of plasmon modes in a nanoparticle does not necessarily coincide with particles size l along the direction of polarization because, for instance, also multipolar modes can be excited in anisotropic particles.[1] Hence, the simplest choice for present calculations consists in assuming that l is equal to the effective radius of the particle d_{eff}:

$$l=d_{eff}=\left(3V_{NP}/4\pi\right)^{1/3} \qquad \text{(m24)}$$

where V_{NP} is particle volume. A similar approximation can be found also in previous works of other authors.[6, 44, 85, 86] Only in case of NSs, for the size correction we considered the thickness of the metal shell as the parameter l.[83]

Acknowledgments

Financial support from University of Padova (PRAT no. CPDA114097/11 and Progetto Strategico STPD11RYPT_001), MIUR (PRIN MULTINANOITA no. 2010JMAZML_001) and "Programma Operativo Nazionale Ricerca e Competitività" 2007-2013, project PAC02L3 00087 SOCIAL-NANO is gratefully acknowledged.

Supporting Information

Definition of σ[400-1200nm] and σ(800nm), spectral dependence of σ_{Abs}, experimental AuFe optical constants.

Bibliography

1) U. Kreibig and M. Vollmer, *Optical Properties of Metal Clusters*, Springer, Berlin, 1995.

2) G. V. Naik, V. M. Shalaev and A. Boltasseva, *Adv Mater,* 2013, 25, 3264-3294.

3) C. F. Bohren and D. R. Huffman, *Absorption and scattering of light by small particles*, Wiley-Interscience, New York, 1983.

4) F. Borghese, P. Denti and R. Saija, *Scattering from model nonspherical particles: theory and applications to environmental physics*, Springer, 2007.

5) J. R. Cole, N. A. Mirin, M. W. Knight, G. P. Goodrich and N. J. Halas, *J. Phys. Chem. C,* 2009, 113, 12090-12094.

6) P. K. Jain, K. S. Lee, I. H. El-Sayed and M. A. El-Sayed, *J. Phys. Chem. B,* 2006, 110, 7238-7248.

7) H. H. Richardson, M. T. Carlson, P. J. Tandler, P. Hernandez and A. O. Govorov, *Nano Lett.,* 2009, 9, 1139-1146.

8) P. K. Jain, X. Huang, I. H. El-Sayed and M. A. El-Sayed, *Acc. Chem. Res.,* 2008, 41, 1578-1586.

9) M. B. Cortie and A. M. McDonagh, *Chem. Rev.,* 2011, 111, 3713-3735.

10) Z. Fang and X. Zhu, *Adv. Mater.,* 2013, 25, 3840-3856.

11) C. Forestiere, A. J. Pasquale, A. Capretti, G. Miano, A. Tamburrino, S. Y. Lee, B. M. Reinhard and L. Dal Negro, *Nano Lett.,* 2012, 12, 2037-2044.

12) M. Lester and D. C. Skigin, *J. Opt.,* 2011, 13, 035105.

13) V. Robbiano, M. Giordano, C. Martella, F. D. Stasio, D. Chiappe, F. B. de Mongeot and D. Comoretto, *Adv. Opt. Mater.,* 2013, 1, 389-396.

14) N. Lagos, M. Sigalas and E. Lidorikis, *Appl. Phys. Lett.,* 2011, 99, 063304.

15) V. Amendola and M. Meneghetti, *Adv. Funct. Mater.,* 2012, 22, 353-360.

16) C. D'Andrea, J. Bochterle, A. Toma, C. Huck, F. Neubrech, E. Messina, B. Fazio, O. M. Marago, E. Di Fabrizio and Lamy de La Chapelle, Marc, *ACS nano,* 2013, 7, 3522-3531.

17) E. Messina, E. Cavallaro, A. Cacciola, R. Saija, F. Borghese, P. Denti, B. Fazio, C. D'Andrea, P. Gucciardi and M. Iati, *J. Phys. Chem. C,* 2011, 115, 5115-5122.

18) B. Metzger, M. Hentschel, T. Schumacher, M. Lippitz, X. Ye, C. B. Murray, B. Knabe, K. Buse and H. Giessen, *Nano Lett.,* 2014, 14, 2867-2872.

19) A. M. Gobin, M. H. Lee, N. J. Halas, W. D. James, R. A. Drezek and J. L. West, *Nano Lett.,* 2007, 7, 1929-1934.

20) Y. Wang, K. C. Black, H. Luehmann, W. Li, Y. Zhang, X. Cai, D. Wan, S. Liu, M. Li and P. Kim, *ACS nano,* 2013, 7, 2068-2077.

21) R. Huschka, A. Barhoumi, Q. Liu, J. A. Roth, L. Ji and N. J. Halas, *ACS nano,* 2012, 6, 7681-7691.

22) J. Huang, K. S. Jackson and C. J. Murphy, *Nano Lett.,* 2012, 12, 2982-2987.

23) S. Mallidi, T. Larson, J. Aaron, K. Sokolov and S. Emelianov, *Opt. Expr.,* 2007, 15, 6583-6588.

24) D. Boyer, P. Tamarat, A. Maali, B. Lounis and M. Orrit, *Science,* 2002, 297, 1160-1163.

25) C. Leduc, J. Jung, R. R. Carney, F. Stellacci and B. Lounis, *ACS nano,* 2011, 5, 2587-2592.

26) B. Lahiri, G. Holland, V. Aksyuk and A. Centrone, *Nano Lett.,* 2013, 13, 3218-3224.

27) K. Ueno, S. Juodkazis, T. Shibuya, Y. Yokota, V. Mizeikis, K. Sasaki and H. Misawa, *J. Am. Chem. Soc.,* 2008, 130, 6928-6929.

28) L. Cao, D. N. Barsic, A. R. Guichard and M. L. Brongersma, *Nano letters,* 2007, 7, 3523-3527.

29) A. Urban, M. Fedoruk, M. Horton, J. Radler, F. Stefani and J. Feldmann, *Nano letters,* 2009, 9, 2903-2908.

30) Z. Fang, Y. Zhen, O. Neumann, A. Polman, García de Abajo, F Javier, P. Nordlander and N. J. Halas, *Nano Lett.,* 2013, 13, 1736-1742.

31) O. Neumann, A. S. Urban, J. Day, S. Lal, P. Nordlander and N. J. Halas, *ACS nano,* 2012, 7, 42-49.

32) O. Neumann, C. Feronti, A. D. Neumann, A. Dong, K. Schell, B. Lu, E. Kim, M. Quinn, S. Thompson, N. Grady, P. Nordlander, M. Oden and N. J. Halas, *Proc. Natl. Acad. Sci. U. S. A.,* 2013, 110, 11677-11681.

33) Z. Fang, Y. Wang, Z. Liu, A. Schlather, P. M. Ajayan, F. H. Koppens, P. Nordlander and N. J. Halas, *Acs Nano,* 2012, 6, 10222-10228.

34) I. Thomann, B. A. Pinaud, Z. Chen, B. M. Clemens, T. F. Jaramillo and M. L. Brongersma, *Nano Lett.,* 2011, 11, 3440-3446.

35) M. L. Brongersma, N. J. Halas and P. Nordlander, *Nat. Nanotech.,* 2015, 10, 25-34.

36) M. W. Knight, H. Sobhani, P. Nordlander and N. J. Halas, *Science,* 2011, 332, 702-704.

37) S. Mukherjee, F. Libisch, N. Large, O. Neumann, L. V. Brown, J. Cheng, J. B. Lassiter, E. A. Carter, P. Nordlander and N. J. Halas, *Nano Lett.,* 2012, 13, 240-247.

38) M. Salmistraro, A. Schwartzberg, W. Bao, L. E. Depero, A. Weber-Bargioni, S. Cabrini and I. Alessandri, *Small,* 2013, 9, 3301-3307.

39) T. Echtermeyer, L. Britnell, P. Jasnos, A. Lombardo, R. Gorbachev, A. Grigorenko, A. Geim, A. Ferrari and K. Novoselov, *Nat. Commun.,* 2011, 2, 458.

40) Z. Fang, Z. Liu, Y. Wang, P. M. Ajayan, P. Nordlander and N. J. Halas, *Nano letters,* 2012, 12, 3808-3813.

41) V. Amendola, O. M. Bakr and F. Stellacci, *Plasmonics,* 2010, 5, 85-97.

42) K. Jiang, D. A. Smith and A. O. Pinchuk, *J. Phys. Chem. C,* 2013, 117, 27073-27080.

43) G. Baffou, R. Quidant and C. Girard, *Appl. Phys. Lett.,* 2009, 94, 153109.

44) K. Park, S. Biswas, S. Kanel, D. Nepal and R. A. Vaia, *J. Phys. Chem. C,* 2014, 118, 5918-5926.

45) M. G. Blaber, M. D. Arnold and M. J. Ford, *J. Phys. D Cond. Matt.,* 2010, 22, 143201.

46) P. K. Jain, K. Manthiram, J. H. Engel, S. L. White, J. A. Faucheaux and A. P. Alivisatos, *Angew. Chem. Int. Ed.,* 2013, 52, 13671-13675.

47) E. Messina, L. D'Urso, E. Fazio, C. Satriano, M. Donato, C. D'Andrea, O. Maragò, P. Gucciardi, G. Compagnini and F. Neri, *J. Quant. Spectr. Rad. Trans.,* 2012, 113, 2490-2498.

48) V. Amendola, S. Scaramuzza, S. Agnoli, S. Polizzi and M. Meneghetti, *Nanoscale,* 2014, 6, 1423-1433.

49) R. Ferrando, J. Jellinek and R. L. Johnston, *Chem. Rev.,* 2008, 108, 845-910.

50) J. Xiao, S. Fan, F. Wang, L. Sun, X. Zheng and C. Yan, *Nanoscale,* 2014, 6, 4345-4351.

51) L. Nie, M. Chen, X. Sun, P. Rong, N. Zheng and X. Chen, *Nanoscale,* 2014, 6, 1271-1276.

52) Y. Yang, J. M. Callahan, T. Kim, A. S. Brown and H. O. Everitt, *Nano Lett.,* 2013, 13, 2837-2841.

53) M. W. Knight, L. Liu, Y. Wang, L. Brown, S. Mukherjee, N. S. King, H. O. Everitt, P. Nordlander and N. J. Halas, *Nano Lett.,* 2012, 12, 6000-6004.

54) V. Amendola, M. Meneghetti, O. M. Bakr, P. Riello, S. Polizzi, D. H. Anjum, S. Fiameni, P. Arosio, T. Orlando, C. de Julian Fernandez, F. Pineider, C. Sangregorio and A. Lascialfari, *Nanoscale,* 2013, 5, 5611-5619.

55) L. Bogani, L. Cavigli, C. de Julián Fernández, P. Mazzoldi, G. Mattei, M. Gurioli, M. Dressel and D. Gatteschi, *Adv. Mater.,* 2010, 22, 4054–4058.

56) G. Armelles, A. Cebollada, A. Garcia-Martin and M. U. Gonzalez, *Adv. Opt. Mater.,* 2013, 1, 2-2.

57) S. Sarina, H. Zhu, E. Jaatinen, Q. Xiao, H. Liu, J. Jia, C. Chen and J. Zhao, *J. Am. Chem. Soc.,* 2013, 135, 5793-5801.

58) J. Suntivich, Z. Xu, C. E. Carlton, J. Kim, B. Han, S. W. Lee, N. Bonnet, N. Marzari, L. F. Allard, H. A. Gasteiger, K. Hamad-Schifferli and Y. Shao-Horn, *J. Am. Chem. Soc.,* 2013, 135, 7985-7991.

59) Y. Lee, Y. Kudryavtsev, V. Nemoshkalenko, R. Gontarz and J. Rhee, *Phys. Rev. B,* 2003, 67, 104424.

60) S. Lal, S. E. Clare and N. J. Halas, *Acc. Chem. Res.,* 2008, 41, 1842-1851.

61) Y. Xia, W. Li, C. M. Cobley, J. Chen, X. Xia, Q. Zhang, M. Yang, E. C. Cho and P. K. Brown, *Acc. Chem. Res.,* 2011, 44, 914-924.

62) M. Choi, R. Bardhan, K. J. Stanton-Maxey, S. Badve, H. Nakshatri, K. M. Stantz, N. Cao, N. J. Halas and S. E. Clare, *Cancer Nano.,* 2012, 3, 47-54.

63) D. C. Adler, S. Huang, R. Huber and J. G. Fujimoto, *Opt. Express,* 2008, 16, 4376-4393.

64) N. Harris, M. J. Ford, P. Mulvaney and M. B. Cortie, *Gold Bull.,* 2008, 41, 5-14.

65) N. J. Hogan, A. S. Urban, C. Ayala-Orozco, A. Pimpinelli, P. Nordlander and N. J. Halas, *Nano Lett.,* 2014, 14, 4640-4645.

66) R. Huschka, J. Zuloaga, M. W. Knight, L. V. Brown, P. Nordlander and N. J. Halas, *J. Am. Chem. Soc.,* 2011, 133, 12247-12255.

67) D. Beaglehole and T. J. Hendrickson, *Phys. Rev. Lett.,* 1969, 22, 133-136.

68) J. Muñoz, M. Lucas, L. Mauger, I. Halevy, J. Horwath, S. Semiatin, Y. Xiao, P. Chow, M. Stone and D. Abernathy, *Phys. Rev. B,* 2013, 87, 014301.

69) S. Bruzzone and M. Malvaldi, *J. Phys. Chem. C,* 2009, 113, 15805-15810.

70) M. D. Arnold and M. G. Blaber, *Opt. Expr.,* 2009, 17, 3835-3847.

71) G. Baffou, R. Quidant and García de Abajo, F Javier, *ACS nano,* 2010, 4, 709-716.

72) F. Borghese, P. Denti, G. Toscano and O. I. Sindoni, *J. Math. Phys.,* 1980, 21, 2754-2755.

73) F. Borghese, P. Denti, R. Saija, G. Toscano and O. I. Sindoni, *Aer. Sci. Technol.,* 1984, 3, 227-235.

74) E. D. Palik, *Handbook of Optical Constants of Solids*, Academic Press, 1985.

75) H. Höchst, P. Steiner and S. Hüfner, *Zeitschrift für Physik B Condensed Matter,* 1980, 38, 201-209.

76) A. A. Wronkowska and A. Wronkowski, *Vacuum,* 1995, 46, 469-471.

77) B. Schmidt and D. W. Lynch, *Physical Review B,* 1971, 3, 4015.

78) H. Koike, S. Yamaguchi and T. Hanyu, *Journal of the Physical Society of Japan,* 1976, 40, 219-225.

79) A. Benhabib, L. Chahed and A. Tadjeddine, *Thin Solid Films,* 1991, 202, 11-19.

80) M. Blaber, M. Arnold, N. Harris, M. Ford and M. Cortie, *Phys. B Cond. Matt.,* 2007, 394, 184-187.

81) P. J. Flatau and B. Draine, *J. Opt. Soc. Am. A,* 1994, 11, 1491.

82) J. Goodman, B. T. Draine and P. J. Flatau, *Opt. Lett.,* 1991, 16, 1198-1200.

83) S. Bruzzone, M. Malvaldi, G. Arrighini and C. Guidotti, *J. Phys. Chem. B,* 2006, 110, 11050-11054.

84) V. Amendola and M. Meneghetti, *J. Phys. Chem. C,* 2009, 113, 4277-4285.

85) C. Noguez, *J. Phys. Chem. C,* 2007, 111, 3806-3819.

86) C. Noguez, *Opt. Mater.,* 2005, 27, 1204-1211.